AIAA JOURNAL
Vol. 43, No. 2, February 2005

Aerodynamic Performance of Transonic Bethe–Zel'dovich–Thompson Flows past an Airfoil

P. Cinnella* and P. M. Congedo†
University of Lecce, 73100 Lecce, Italy

Dense gasdynamics studies the flow of gases in the thermodynamic region above the upper saturation curve, close to the liquid-vapor critical point. In recent years, great attention has been paid to certain substances, known as the Bethe–Zel'dovich–Thompson (BZT) fluids, which exhibit negative values of the fundamental derivative of gasdynamics for a whole range of temperatures and pressures in the vapor phase. This can lead to nonclassical gasdynamic behaviors, such as rarefaction shock waves, mixed shock/fan waves, and shock splitting. The uncommon properties of BZT fluids can find practical applications, for example, in the reduction of losses as a result of wave drag and shock/boundary-layer interaction in organic Rankine cycle turbines. The present work provides a detailed numerical study of transonic BZT fluid flows past a simplified configuration, represented by an isolated NACA0012 airfoil. The objective is to investigate the influence of BZT effects on the airfoil performance (specifically on the lift-to-drag ratio).

I. Introduction

DENSE gasdynamics studies the dynamic behavior of gases at thermodynamic conditions close to the liquid/vapor critical point, where the perfect gas law is invalid. In the dense regime, some heavy polyatomic fluids, referred to as the Bethe–Zel'dovich–Thompson (BZT) fluids, can exhibit nonclassical nonlinearities, such as expansion shock waves, mixed shock/fan waves, and splitting shocks.[1–3] These anomalies occur when the fundamental derivative of gasdynamics[1]

$$\Gamma := \frac{v^3}{2a^2}\left(\frac{\partial^2 p}{\partial v^2}\right)_s = 1 + \frac{\rho}{a}\left(\frac{\partial a}{\partial \rho}\right)_s \tag{1}$$

exhibits a region of negative values, between the upper saturation curve and the $\Gamma = 0$ contour. In the preceding equation, v is the fluid specific volume, p the pressure, s the entropy, $\rho = 1/v$ the density, and a is the sound speed. Such a region is often referred to as the *inversion zone*, and the $\Gamma = 0$ contour is called the *transition line*. The fundamental derivative Γ can be interpreted as a measure of the rate of change of the sound speed with density in isentropic perturbations. If $\Gamma < 1$, the flow will exhibit an uncommon sound speed variation in isentropic perturbations: a grows in isentropic expansions and decreases in isentropic compressions, the opposite of what happens in "common" fluids. For perfect gases, Γ is equal to $(\gamma + 1)/2$, where the specific heats ratio γ is always greater than 1 for thermodynamic stability reasons; therefore, $\Gamma > 1$ as well.

The sign of Γ is univocally determined by the sign of the second derivative $(\partial^2 p/\partial v^2)_s$, that is, by the concavity of constant entropy lines (isentropes) in the p–v plane. Now, it is well known that isentropes tend to coincide with isotherms as the fluid specific heats approach infinity. In the dense regime, the perfect-gas law is no longer valid, and more complex equations of state have to be considered to model the thermodynamic behavior of the gas. For such equations, the isotherms are no longer positively concave hyperboles in the p–v plane. Instead, they are more complicated curves that exhibit negative concavity in the neighborhood of the upper saturation curve, in order to satisfy the thermodynamic conditions of zero slope and zero curvature at the critical point. Therefore, any fluid with sufficiently large specific heats will also have negatively concave isentropes in the dense-gas region of the p–v plane, which implies $\Gamma < 0$ in the same region. Figure 1 illustrates the inversion zone and transition line for a BZT van der Waals gas. Two isentropes and the critical isotherm are also represented. The isentrope closer to the saturation curve exhibits reversed concavity within the inversion zone. The existence of fluids with a negative fundamental derivative in the single-phase region above the upper saturation curve has been demonstrated, using accurate thermodynamic data, by Lambrakis and Thompson,[4] Thompson and Lambrakis,[5] and Cramer.[6] Examples of BZT fluids are given by heavy hydrocarbons (decane or higher), commercially available heat-transfer fluids such as FC-71 ($C_{18}F_{39}N$), FC-72 (C_6F_{14}), PP9 ($C_{11}F_{20}$), PP10 ($C_{13}F_{22}$), and some methylsiloxanes.

The dynamics of Bethe–Zel'dovich–Thompson fluids has been studied extensively in recent years. We refer to the work by Cramer[7] and Menikoff and Plohr[8] and the references cited therein for more details about nonclassical waves in dense gas flows. The most impressive phenomenon is the disintegration of compression shocks in fluids with $\Gamma < 0$. The entropy change through a weak shock can be written as[2]

$$\Delta s = -(a^2\Gamma/v^3)[(\Delta v)^3/6T] + \mathcal{O}[(\Delta v)^4] \tag{2}$$

where Δ represents a change in a given fluid property through the shock and T is the absolute temperature. If $\Gamma < 0$, the second law of thermodynamics requires that compression shocks (characterized by a negative change in the specific volume) cannot form and necessarily split into fans if inserted within the flow. Conversely, expansion shock waves are physically admissible! In practice, Γ rarely has constant negative sign throughout the flow because of the finite extent of the inversion zone. At the crossing of the transition line, where Γ equals zero, the genuine nonlinearity of the flow characteristic fields is lost,[8] and nonclassical waves can be generated, such as mixed shock-fan waves and splitting shocks. For example, it can happen that a compressive wave would start in the positive Γ region as a shock, and then split into a compression fan as the flow enters the inversion zone. This results in discontinuities of limited strength for thermodynamic conditions where $\Gamma \approx 0$. Cramer and Kluwick[2] showed that $\Gamma = \mathcal{O}(\Delta v)$ for small volume changes in the vicinity of the transition line. Thus, from Eq. (2) it results that shock waves having jump conditions in the thermodynamic region near the $\Gamma = 0$ contour are one order of magnitude weaker than normal.

The nonclassical phenomena typical of BZT fluids have several practical outcomes; prominent among them is an active research

Received 27 February 2004; revision received 24 May 2004; accepted for publication 17 June 2004.

*Assistant Professor, Department of Engineering for Innovation, via Monteroni. Member AIAA.

†Ph.D. Student, Department of Engineering for Innovation, via Monteroni.

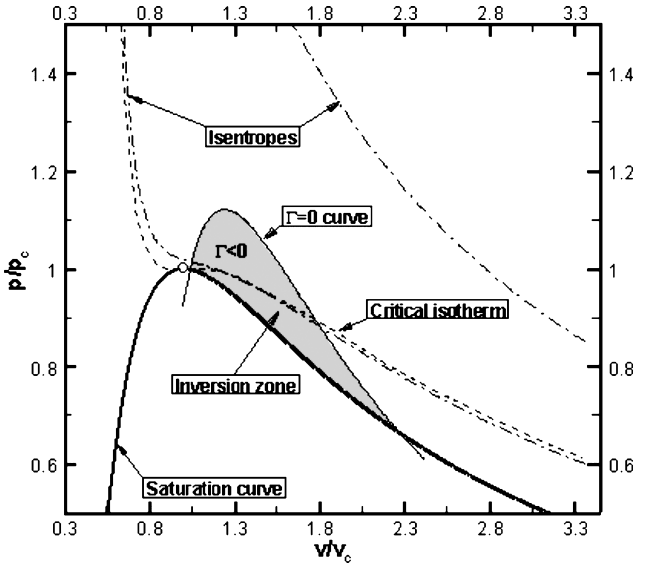

Fig. 1 Amagat diagram for a van der Waals gas with $\gamma = 1.0125$.

effort to reduce losses caused by wave drag and shock/boundary-layer interactions in turbomachines and nozzles,[9–12] with particular application to organic Rankine cycles (ORCs). ORCs are used to generate electric energy in low-power applications. They typically utilize a low-temperature heat source, such as geothermal and solar sources, or waste heat from industrial applications, and a single expansion stage, which operates in the transonic/supersonic regime. One of the major loss mechanisms in transonic and supersonic turbomachinery is related to the generation of shock waves. In addition to irreversibilities associated with the shock waves themselves, additional losses can occur because of shock/boundary-layer interactions, leading to boundary-layer transition and separation. On the other hand, ORCs' working fluids are heavy organic compounds with large heat capacities, which, in many cases, possess BZT properties. The use of a BZT fluid could avoid shock formation and, ideally, allow isentropic turbine expansion. However, simply utilizing a BZT working fluid is not sufficient to maximize the reduction in losses: it is also necessary to operate the turbine cascade at a pressure and temperature near the inversion zone. But, how near? Previous works on BZT transonic flows past airfoils[10] and on BZT flows through turbine cascades,[11,12] generally considered operation conditions in the very neighborhood of the $\Gamma = 0$ curve, just above the upper saturation curve. In such conditions, the flowfield evolves almost entirely within the inversion zone, and no compressive shock waves are formed. The result is an almost isentropic expansion through the entire cascade. Unfortunately, the inversion zone has a quite limited extent. Therefore, a reduction in the temperature jump between the heater and condenser stages is generally needed in order to operate the turbine cascade in the BZT regime. However, if the temperature jump is taken too small, the overall cycle efficiency tends to decrease, the efficiency of power cycles being limited by the efficiency of the ideal Carnot cycle:

$$\eta_{\text{Carnot}} = 1 - \frac{T_{\text{condenser}}}{T_{\text{heater}}}$$

In summary, the risk is to enhance turbine efficiency at the cost of a lower global cycle power output. The optimum choice depends basically on the fluid properties (extent of the inversion zone) and on the blade geometry. An overview of difficulties related with the development of BZT organic Rankine cycles has been provided in Ref. 13.

An alternative approach, largely unexplored until now, is to allow the flow to evolve in part outside the inversion zone. With this choice, compression shocks and mixed waves can occur, causing losses. However, such waves are expected to be relatively weak, if they have jump conditions in the vicinity of the transition line.[2] This means that the associated losses will be lower than normal, leading to high turbine efficiency. On the other hand, the choice to operate the turbine cascade partially outside the inversion zone allows an increase in the temperature jump of the power cycle, thus alleviating the difficulties described above.

The objective of the present research is to explore the feasibility of such an approach, providing (for the first time, to the best of the authors' knowledge) a detailed parametric investigation of the effect of the operating conditions on the aerodynamic performance of turbine blades. More specifically, the present paper investigates how dense gas effects influence the aerodynamic performance (lift, drag, lift-to-drag ratio) of a simplified configuration, represented by an isolated NACA0012 airfoil in the transonic regime. The freestream thermodynamic state is changed, starting from operation points located in the neighborhood of the transition line and adjacent to the vapor saturation curve, and progressively increasing the freestream pressure and temperature until BZT effects disappear from the flow. As BZT phenomena mainly influence the inviscid flow behavior, we restrict our analysis to the Euler equations. The computations are performed using the van der Waals equation of state for polytropic gases, the simplest thermodynamic model accounting for BZT effects. Such a model is computationally inexpensive and has been often utilized to provide a qualitative description of BZT fluid flows.[9,14–16]

The paper is organized as follows. In Sec. II, the governing equations are presented. A brief description of the van der Waals thermodynamic model is provided, and its relevance for the analysis of BZT flows is discussed, as well as potential sources of error. Section III provides the details of the numerical method. Finally, Sec. IV provides numerical results for the transonic BZT flows past a NACA0012 airfoil. Specifically, three nonlifting cases are investigated first. The results compare well with existing theoretical results[10] and provide further insight into some complex flow features. Then, several lifting cases are considered, in order to investigate how BZT effects affect the airfoil performance, as well as the influence of the freestream kinematic and thermodynamic conditions on the lift-to-drag ratio of the airfoil.

II. Governing Equations and Thermodynamic Model

The present work deals with inviscid compressible flows of dense gases, governed by the Euler equations. Because we are interested in finite volume solutions of the governing equations, we consider a system of conservation laws written in integral form for a control volume Ω with boundary $\partial\Omega$:

$$\frac{\mathrm{d}}{\mathrm{d}t}\int_{\Omega} w \,\mathrm{d}\Omega + \int_{\partial\Omega} \boldsymbol{f}\cdot\boldsymbol{n}\,\mathrm{d}S = 0 \tag{3}$$

In Eq. (3), w is the conservative variable vector,

$$w = (\rho, \rho\boldsymbol{v}, \rho E)^T$$

$\boldsymbol{n}$ is the outer normal to $\partial\Omega$, and $\boldsymbol{f}$ is the flux vector

$$\boldsymbol{f} = (\rho\boldsymbol{v},\ p\bar{\bar{I}} + \rho\boldsymbol{v}\boldsymbol{v},\ \rho\boldsymbol{v}H)^T$$

In these equations, ρ is the fluid density, $\boldsymbol{v}$ is the velocity vector, E the specific total energy, $H = E + p/\rho$ the specific total enthalpy, and $\bar{\bar{I}}$ the unit tensor. The preceding equations should be completed by an equation of state, assumed to be of the form

$$p = p[\rho(w), e(w)] \tag{4}$$

with e being the specific internal energy. In the present work, the van der Waals equation of state for polytropic gases is considered. Such an equation relates the fluid pressure to the specific internal energy and the fluid density through the formula

$$p = (\gamma - 1)\frac{\rho e + \alpha\rho^2}{1 - \rho\beta} - \alpha\rho^2 \tag{5}$$

where γ is the (constant) specific heat ratio and α and β are two gas-dependent parameters, related to the fluid critical values by the conditions:

$$\alpha = \frac{9p_c}{8\rho_c^2 Z_c}, \qquad \beta = \frac{1}{3\rho_c}$$

where $Z_c = p_c/(R\rho_c T_c)$ is the critical compressibility factor, equal to $\frac{3}{8}$ for a van der Waals gas; and p_c, ρ_c, and T_c are the critical pressure, density, and temperature, respectively. Normalizing the equations with respect to the critical values, one finds that, for a generic van der Waals gas, the normalized van der Waals constants are

$$\alpha = 3, \qquad \beta = \tfrac{1}{3}$$

The van der Waals gas model represents the earliest attempt to correct the perfect-gas law in order to take into account covolume effects and attractive intermolecular forces. It satisfies only two thermodynamic constraints: the horizontal slope and inflection of the critical isotherm at the critical point. However, these are sufficient conditions that make the van der Waals equation capable to model BZT fluid behavior. In fact, in the limit $c_v/R \to \infty$, γ tends to one, and the isentropes and isotherms coincide. Therefore, a van der Waals gas with sufficiently high c_v/R ratio is expected to exhibit reversed isentrope concavity above the upper saturation curve: it possesses BZT properties. It is possible to show[5] that, taking the specific heat ratio γ in the range

$$1 < \gamma \leq 1.06$$

a region of negative values of the fundamental derivative appears. Figure 1 shows the p–v diagram and the inversion zone for a van der Waals gas with $\gamma = 1.0125$. In Ref. 5, predictions provided by the van der Waals equation on the extent of the inversion zone for a given gas are compared with other equations of state. In particular, the comprehensive equation of state of Martin and Hou,[17] involving five virial terms and satisfying 10 thermodynamic constraints, is considered. Such equation is one of the best available gas models to manageably compute dense gas effects.[18] The extent of the inversion zone predicted by the van der Waals equation for a gas with $c_v/R \cong 20$ is nearly the same as that predicted by the Martin–Hou equation for a gas with $c_v/R \cong 80$ (with c_v taken as the ideal-gas specific heat at constant volume at the critical point). Therefore, the van der Waals equation largely overestimates the extent of the inversion zone. However, if this inaccuracy affects quantitative results obtained for a given gas, it does not affect the qualitative behavior significantly: the results obtained are roughly representative of the thermodynamic response of a real-world BZT gas with higher specific heats.

III. Numerical Method

The governing equations are discretized using a recently developed cell-centered finite volume scheme of third-order accuracy,[19] extended to the computation of flows with an arbitrary equation of state.[20] The main features of the algorithm are presented for the case of the one-dimensional Euler equations written in conservation form:

$$\frac{\partial w}{\partial t} + \frac{\partial f(w)}{\partial x} = 0 \tag{6}$$

with $w = (\rho, \rho u, \rho E)^T$ being the conservative variable vector and $f(w) = (\rho u, \rho u^2 + p, \rho u H)^T$ the flux function. System (6) is approximated by a conservative, semidiscrete scheme of the form

$$\left.\frac{\partial w}{\partial t}\right|_j + \frac{(\delta h)|_j}{\delta x} = 0 \tag{7}$$

where δx is the space increment, j is a given mesh point, h is a numerical flux, and δ is the difference operator for one cell:

$$(\delta\cdot)|_{j+\frac{1}{2}} = (\cdot)|_{j+1} - (\cdot)|_j$$

The flux function at the interface between two adjacent cells is approximated through the fourth-order-accurate centered zero-dissipative numerical flux:

$$h_{j+\frac{1}{2}} = (\mu f)|_{j+\frac{1}{2}} - \tfrac{1}{6}(\delta^2 \mu f)|_{j+\frac{1}{2}} \tag{8}$$

where the average operator for one cell μ is defined by

$$(\mu\cdot)|_{j+\frac{1}{2}} = \left[(\cdot)|_j + (\cdot)|_{j+1}\right]\Big/2$$

To ensure stability and avoid numerical oscillations, a dissipation term has to be added. A possible choice is a blend of second- and fourth-order derivatives.[21] This leads to the dissipative numerical flux:

$$h_{j+\frac{1}{2}} = (\mu f)|_{j+\frac{1}{2}} - \tfrac{1}{6}(\delta^2 \mu f)|_{j+\frac{1}{2}} - \left[\varepsilon_2 \rho(A)(\delta w) - \varepsilon_4 \rho(A)(\delta^3 w)\right]\Big|_{j+\frac{1}{2}} \tag{9}$$

where $\rho(A) = |u| + a$ is the spectral radius of the flux Jacobian matrix $A = \partial f/\partial w$, with the sound speed a given by

$$a = \left(\frac{p}{\rho^2}\frac{\partial p}{\partial e} + \frac{\partial p}{\partial \rho}\right)^{\frac{1}{2}} \tag{10}$$

$$\varepsilon_2|_{j+\frac{1}{2}} = k_2 \max\{\nu_j, \nu_{j+1}\}, \qquad \varepsilon_4|_{j+\frac{1}{2}} = \max\left\{0, k_4 - \varepsilon_2|_{j+\frac{1}{2}}\right\}$$

$$\nu_j = \left|\frac{p_{j+1} - 2p_j + p_{j-1}}{p_{j+1} + 2p_j + p_{j-1}}\right|$$

In the preceding equation, k_2 and k_4 are constant parameters, taken equal to 0.5 and 0.016 for all of the computations presented in the following. The dissipation term is $\mathcal{O}(\delta x^3)$ in smooth flow regions, so that the dissipative numerical flux is third-order accurate. The use of a scalar dissipation term simplifies the scheme implementation when highly complex equations of state are employed and greatly reduces the overall computational cost.

The preceding scheme can be interpreted as a third-order extension of the classical Jameson scheme,[21] of second-order accuracy. Specifically, the high-order scheme can be derived by correcting the truncation error leading term, representing a dispersion error, of Jameson's scheme. Correction of the dispersion error term reduces the scheme's tendency to produce spurious oscillations close to flow discontinuities. On the other hand, the dissipative error is also reduced: if the scheme tends to give less oscillatory solutions, the second-order nonlinear dissipation term in Eq. (9), which becomes important in regions where oscillations tend to appear, will remain small. The very low intrinsic dissipation of the third-order centered scheme has been confirmed by numerical results.[19,20,22]

The numerical method is extended to multidimensional structured meshes through a cell-centered finite volume formulation. To preserve the high accuracy of the scheme on irregular grids, the numerical fluxes are evaluated using suitably weighted discretization formulas, which take into account mesh deformations: this ensures third-order accuracy on moderately deformed meshes and at least second-order accuracy on highly distorted meshes (see Ref. 23 for details). The governing equations are integrated in time using a four-stage Runge–Kutta scheme.[21] Local time-stepping, implicit residual smoothing, and multigrid strategies are used to efficiently drive the solution to the steady state.

IV. Results

A. Code Validation

The numerical method described has been successfully validated for a variety of both perfect- and real-gas flows.[19,20,22] Here we report as an example the propagation of nonclassical waves in a dense gas shock tube. For this problem, numerical results provided by the present method can be compared with those obtained by Argrow[14] and Guardone and Vigevano.[24] The left and right initial conditions (nondimensionalized by means of the critical density

Table 1 Initial data for the dense gas shock tube

Quantity	Value
ρ_l	0.879
u_l	0
p_l	1.090
Γ_l	−0.031
ρ_r	0.275
u_r	0
p_r	0.575
Γ_r	0.703

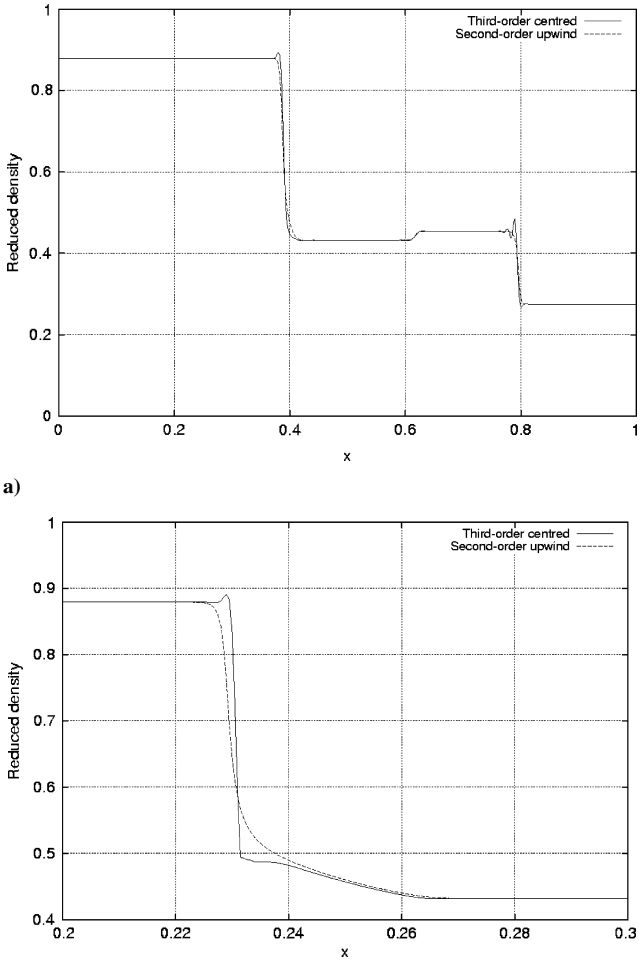

Fig. 2 Dense gas shock tube: a) density distribution at $t^* = 0.2$, $\Delta t = 10^{-3}$, 400-cell grid; and b) enlargement of the mixed rarefaction wave, $t^* = 0.48$, 1000-cell grid.

and pressure) are reported in Table 1. The solution is characterized by a left-running mixed expansion wave, composed by an expansion shock and a rarefaction fan, a middle contact discontinuity, and a right-running compression shock. Figure 2a presents the density distribution computed at nondimensional time $t^* = 0.2$, on a computational grid composed of 400 cells. The present third-order centered method is compared with a second-order upwind solver.[24] The two solutions are very similar and agree with those provided in Refs. 14 and 24. Figure 2b presents an enlargement of the transition from continuous to discontinuous expansion (computed at $t^* = 0.48$ on a grid composed by 1000 cells). The third-order scheme gives a quite sharp transition, whereas in the upwind scheme solution the transition point cannot be detected as clearly.

B. BZT Flows past a NACA0012 Airfoil

In the present section, the steady inviscid flow over a NACA0012 airfoil in transonic regime is considered, and several flow conditions are taken into account. First, nonlifting flows are studied, for different values of the freestream conditions (Mach number, pressure, and density). The results are compared with those obtained for a perfect gas in order to highlight the peculiarities of BZT flows. Moreover, the present results are compared, at least qualitatively, with those provided in Ref. 10, where the transonic small-disturbance potential equation was solved.

For nonlifting cases, the computations are performed using three half-grids of increasing density, formed by 68×20, 136×40, and 272×80 cells, respectively. The finer and the coarser grid have been generated by doubling and halving, respectively, the number of cells of the medium one (in each direction). The outer boundary is about 20 chords away from the airfoil, and the mean height of the first cell closest to the wall is about 5×10^{-2} chords on the medium grid. A view of the coarse grid is provided in Fig. 3.

Table 2 summarizes the conditions chosen for this first series of numerical experiments. The two test cases indicated as PFGx, with x a number, concern the flow of a perfect diatomic ($\gamma = 1.4$) gas. The three test cases denoted as DGx all involve dense gas phenomena. The working fluid is a heavy polytropic van der Waals gas with $\gamma = 1.0125$. The pressure and density values in the far field (normalized with respect to their critical point values) are selected in order to have both positive and negative values of Γ.

The PFG1 case concerns a flow with freestream Mach number equal to 0.85 and zero angle of attack. The flow is characterized by symmetric strong shock waves at about 85% of the chord. Contours of the pressure coefficient

$$C_p := \frac{p - p_\infty}{\frac{1}{2}\rho_\infty V_\infty^2}$$

obtained on the finer grid, are represented in Fig. 4. In the preceding equation, p_∞, ρ_∞, and V_∞ are the freestream pressure, density, and velocity, respectively. Figures 5a and 5b show the variation along

Table 2 Test case description

Case	p_∞/p_c	ρ_∞/ρ_c	Γ_∞	M_∞
PFG1	$\ll 1$	$\ll 1$	$(\gamma+1)/2$	0.850
DG1	1.07	0.920	0.143	0.850
PFG2	$\ll 1$	$\ll 1$	$(\gamma+1)/2$	0.998
DG2	1.07	0.920	0.143	0.998
DG3	0.944	0.600	−4.39e–2	0.998

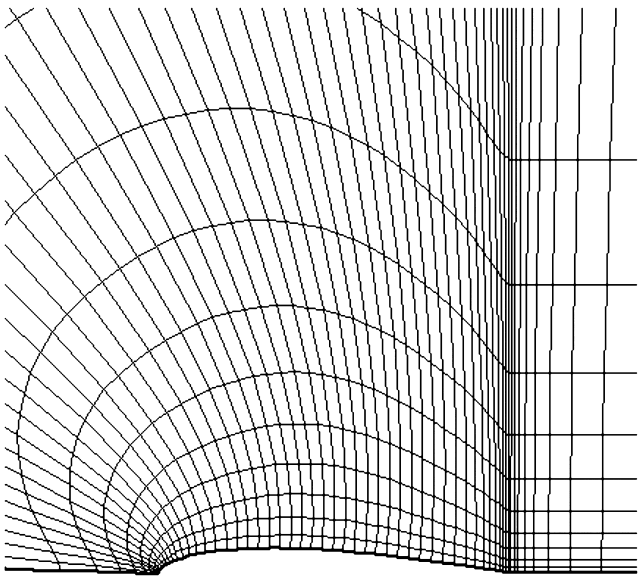

Fig. 3 Partial view of the coarse grid.

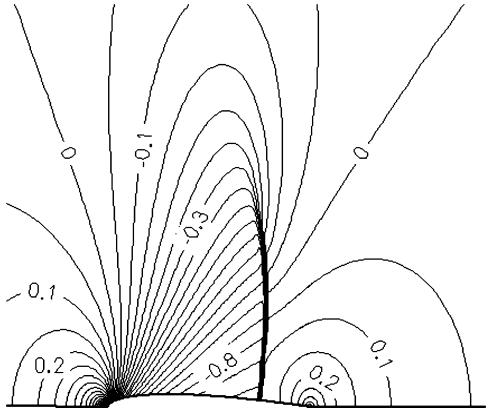

Fig. 4 Case PFG1: transonic perfect-gas flow past a NACA0012 with $M_\infty = 0.85$, $\alpha = 0$ deg. Pressure coefficient contours: $\Delta C_P = 0.05$.

the airfoil of the pressure coefficient and the Mach number on the three grids. Grid convergence is obtained on the medium grid. The entropy error, $\Sigma := (s - s_\infty)/s_\infty$, generated at the airfoil leading edge, is also reported in Fig. 5c, showing the very low intrinsic dissipation of the numerical scheme. In particular, the entropy error upstream of the shock is $\mathcal{O}(10^{-6})$ on the fine grid. Even if not reported, similar or lower errors have been found for the dense gas cases presented in the following. For a more uniform reporting of the grid convergence, the scheme's order of convergence is estimated following Roache's method,[25] based on Richardson extrapolation. Given three numerical solutions computed on grids of increasing spacing, with constant grid-refinement ratio r, the actual order of convergence is

$$p = \ell_n[(f_3 - f_2)/(f_2 - f_1)]/\ell_n(r)$$

where f is a solution functional and indices 1 and 3 are referred to the finer and the coarser grid solution, respectively. A computed order of convergence of 2.2, based on the drag coefficient C_D, has been found for the present computation, against a theoretical order of convergence of 3. The estimated order of convergence can be used to compute Roache's grid convergence index (GCI) on the finer and medium grid, which represents an estimate of how far the numerical solution is from its asymptotic value. GCIs of 0.08 and 0.39% have been found for the finer and the medium grid, respectively, indicating that the solution is well within the asymptotic range. Such values are likely to be conservative.[25]

The DG1 test case has a freestream Mach number identical to the one used for the perfect-gas computation. However, for a BZT van der Waals gas with freestream thermodynamic conditions close to the transition zone, the fundamental derivative drops to negative values at the very beginning of the expansion past the airfoil leading edge: consequently, the sound speed increases, and the flow does not become supersonic as in the perfect-gas case. In fact, an examination of the flow isobars (Fig. 6) and the Mach distribution at the wall (Fig. 7) shows that the flow is subsonic everywhere. Figure 7 also shows the distributions of the pressure coefficient and the fundamental derivative at the wall. At the leading edge, the flow pressure is isentropically raised to its stagnation value, while the fundamental derivative increases. However, when the flow accelerates turning around the airfoil nose, the pressure drops significantly. Thus, the fundamental derivative decreases and reaches negative values as the flow crosses the transition line. As Γ becomes smaller than 1, the sound speed reverses its behavior and begins to increase. Consequently, the Mach number first grows at a lower rate, and then begins to drop, in spite of the still falling pressure. In summary, because of the uncommon sound speed variation typical of BZT gases, the flow remains entirely subsonic, and no discontinuities appear. To evaluate the solution accuracy for dense gas computations, a grid-convergence study has been performed, as in the previous perfect-gas case. Grid convergence for the wall pressure coefficient and Mach number has been obtained on the medium grid. For this

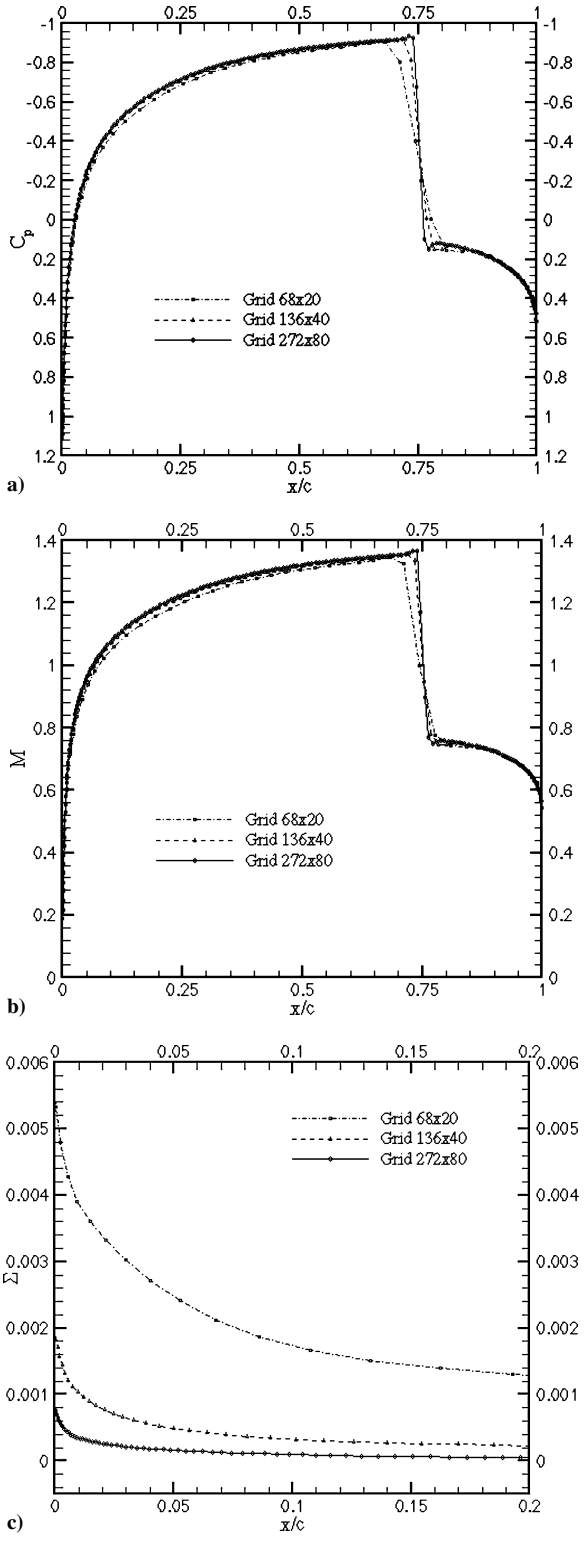

Fig. 5 Case PFG1: a) pressure coefficient, b) Mach number, and c) entropy error at the wall.

shock-free problem, the computed convergence order of the numerical method is found to be equal to 2.5. GCIs, based on the lift coefficient, are equal to 0.68% on the fine grid and 3.8% on the medium one, the solution being within the asymptotic range. For all of the computations presented next, except case DG3 that will be discussed later, grid convergence for the wall pressure and Mach number was obtained on the medium grid. However, the results presented in the following have been obtained on the fine grid, unless stated otherwise.

To obtain supercritical flow conditions, the freestream Mach number has to be raised. An estimate of the critical Mach number for

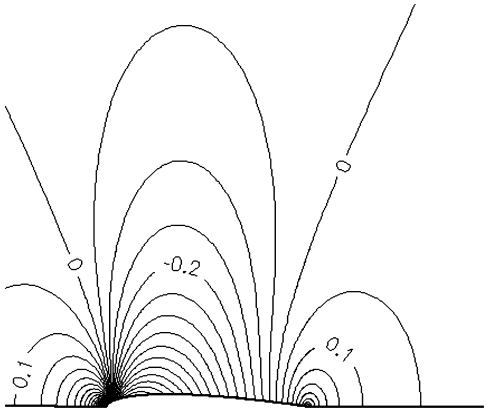

Fig. 6 Case DG1: BZT flow past a NACA0012 with $M_\infty = 0.85$, $\alpha = 0$ deg, $\Gamma_\infty = 0.143$. Pressure contours: $\Delta C_P = 0.05$.

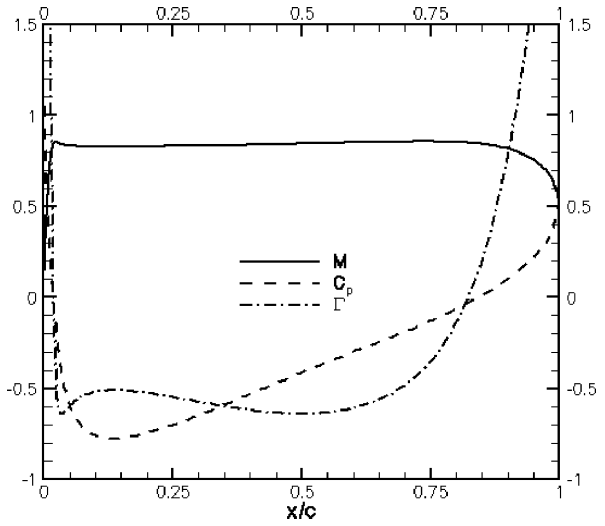

Fig. 7 Case DG1: Mach number, pressure coefficient, and fundamental derivative at the wall.

BZT flows past thin airfoils has been found[10]:

$$M_{\rm cr} \cong 1 - \tfrac{1}{2}\left(\Gamma_\infty^2 \big/ \Lambda_\infty\right)$$

where

$$\Lambda_\infty = \rho_\infty \frac{\partial \Gamma}{\partial \rho}(\rho_\infty, s_\infty)$$

is the second (cubic) nonlinearity parameter introduced by Cramer and Kluwick.[2] For the freestream conditions of case DG1, the critical Mach number is about 0.99.

For the DG2 test case the freestream thermodynamic conditions are unchanged with respect to DG1, but a freestream Mach number equal to 0.998 has been chosen in order to obtain supercritical flow. In such conditions, a very weak expansion shock forms at about 10% of the chord, followed by a weak compression shock at about 90% of the chord. Both shocks are almost sonic upstream. Figures 8 and 9 show the flow isobars for a perfect-gas flow (case PFG2) with $M_\infty = 0.998$ and for case DG2. The perfect-gas flow is characterized by a very strong compression shock close to the trailing edge, with upstream Mach number about equal to 1.5. Mach number, pressure coefficient, and fundamental derivative at the wall for case DG2 are provided in Fig. 10.

The last test case DG3 has freestream thermodynamic conditions in the negative Γ region, close to the low-density branch of the transition line. Such a choice leads to the formation of a bow shock upstream of the airfoil, because of dropping sound speed for increasing pressure, which makes the flow supersonic upstream of the

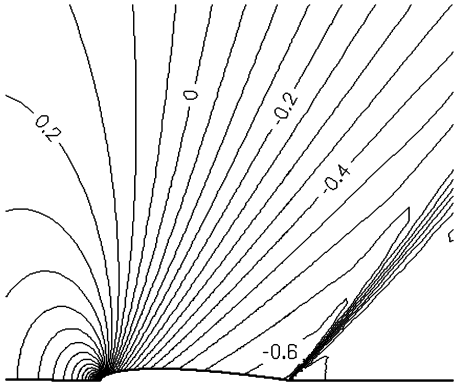

Fig. 8 Case PFG2: perfect-gas flow past a NACA0012 with $M_\infty = 0.998$, $\alpha = 0$ deg. Pressure contours: $\Delta C_P = 0.05$.

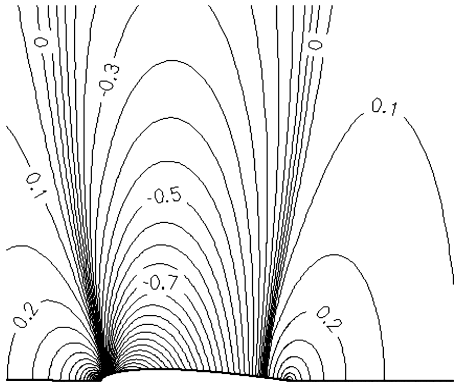

Fig. 9 Case DG2: BZT flow past a NACA0012 with $M_\infty = 0.998$, $\alpha = 0$ deg, $\Gamma_\infty = 0.143$. Pressure contours: $\Delta C_P = 0.05$.

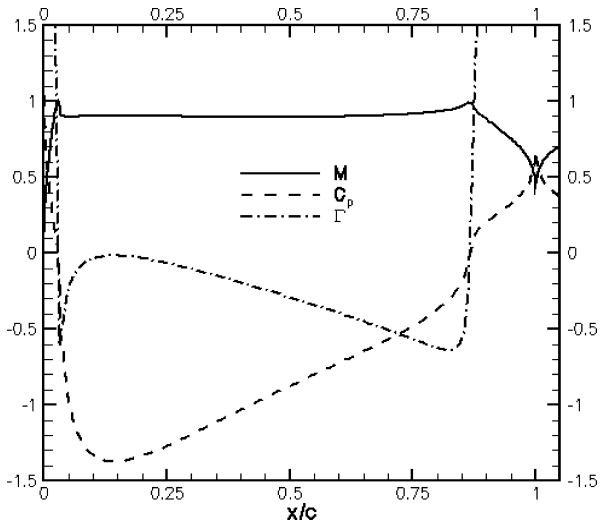

Fig. 10 Case DG2: Mach number, pressure coefficient, and fundamental derivative at the wall.

airfoil leading edge (Fig. 11). To obtain a grid-converged solution downstream of the airfoil (where an expansion shock forms), an extremely fine grid of 624×160 cells was employed. We now describe the evolution of a fluid particle moving along the stagnation streamline. Approaching the airfoil, the particle is compressed. During such compression, Γ shifts from its negative freestream value to positive values. At the same time, as $\Gamma < 1$ the sound speed falls, and the flow becomes supersonic: in such conditions, a compression bow shock forms upstream of the airfoil nose. Downstream of the bow shock, the flow is subsonic and compresses isentropically to stagnation conditions. The flow then expands again turning around

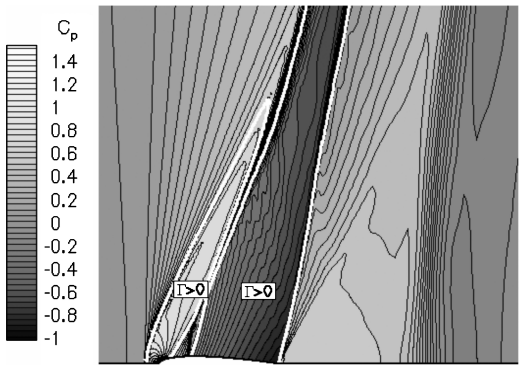

Fig. 11 Case DG3: BZT flow past a NACA0012 with $M_\infty = 0.998$, $\alpha = 0$ deg, $\Gamma_\infty = -0.0439$. Pressure contours: $\Delta C_P = 0.05$. Thick white lines represent $\Gamma = 0$ contours.

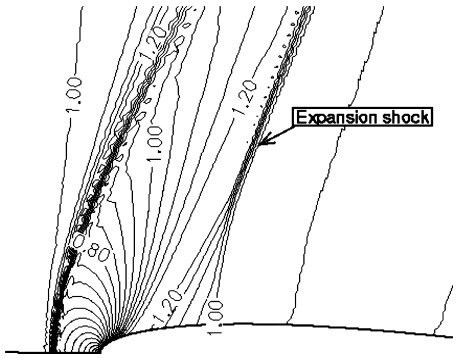

Fig. 12 Case DG3: Detail of the iso-Mach contours close to the wall with $\Delta M = 0.05$.

the airfoil leading edge: consequently, Γ reverses its sign, and, as the flow is deflected by a convex wall, an expansion shock forms. Figure 12 presents a closeup of the solution near the wall, showing the coalescence of the flow Mach lines, and the formation of the expansion shock. In fact, the fundamental derivative Γ is related to the slope μ of the Mach lines as follows[1]:

$$\mathrm{d}(\Theta + \mu) = \frac{\Gamma M^2}{M^2 - 1}\,\mathrm{d}\Theta$$

where Θ is the flow deflection angle. If Γ is negative, the Mach lines will become steeper during flow expansions past convex walls. At the airfoil trailing edge, a mixed compression-shock/compression-fan-wave forms, followed by a second expansion shock about 1.5 chords downstream of the trailing edge. In Fig. 11 the $\Gamma = 0$ contours are represented. Flow regions characterized by positive Γ have a finite extent, as Γ should recover a negative value in the freestream. Consequently, the bow shock ends at a finite distance from the wall. Figure 11 also shows that the bow shock is preceded by a continuous compression. Thus, the compression wave upstream of the leading edge should be more properly seen as a mixed wave. Such a wave degenerates into a continuous compression wave sufficiently far away from the wall, where it interacts with the expansion shock. The two waves finally cancel each other. Figure 13 presents the pressure, Mach, and Γ distribution along the stagnation streamline. Present results are in qualitative agreement with those shown in Ref. 10 for a circular arc airfoil. However, the results in Ref. 10 were obtained by solving a simplified model (the small perturbation potential equation for thin airfoils), and using relatively coarse grids, so that many flow details could not be clearly observed.

The next series of results concerns lifting cases. The computations are performed using a set of three symmetric C grids of increasing density (136×20, 272×40, and 544×80 cells). Such grids have been obtained by doubling symmetrically the half-grids used for the previous test cases.

Firstly, the airfoil angle of attack is changed at a fixed freestream Mach number, pressure, and density: these are the same of case

Table 3 Lift vs incidence: $M_\infty = 0.85$, $p_\infty/p_c = 1.07$, $\rho_\infty/\rho_c = 0.92$

α,deg	C_L
1	0.192
3	0.622
5	1.07

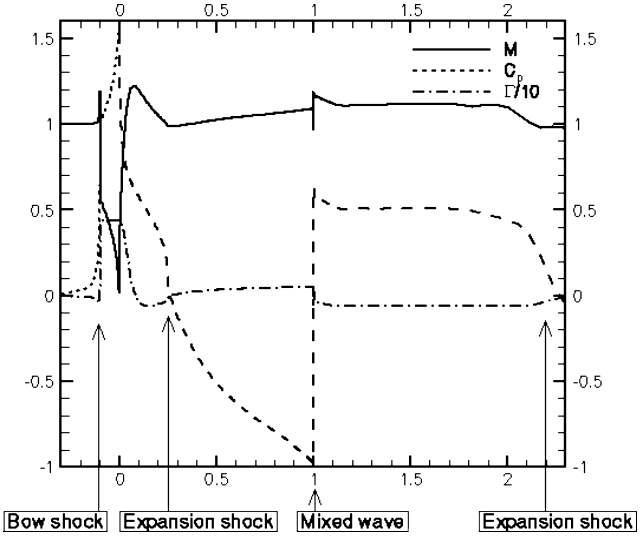

Fig. 13 Case DG3: Mach, pressure coefficient, and fundamental derivative distribution along the wall streamline.

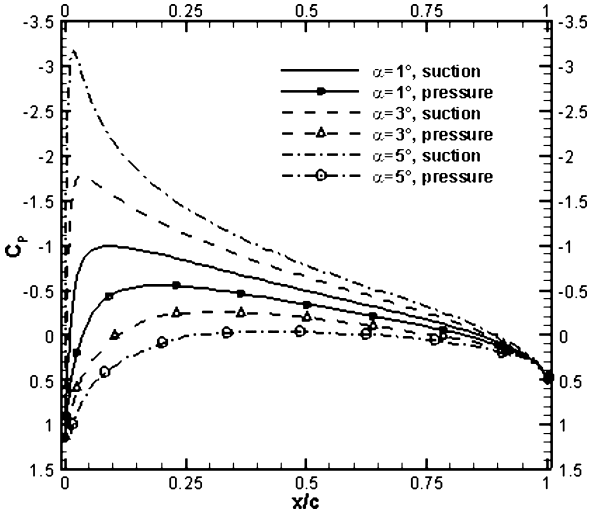

Fig. 14 BZT flow past a NACA0012 with $M_\infty = 0.85$, $\Gamma_\infty = 0.143$. Wall pressure coefficient for different values of the angle of attack.

DG1. Angles of 1, 3, and 5 deg are considered. In each of the three cases, the flow remains subsonic. As the freestream is uniform and steady and viscous effects are neglected, the drag coefficient is expected to be zero. However, because of numerical dissipation C_D takes small nonzero values, of the order of 10^{-4} on the fine grid. Table 3 shows the lift coefficient variation vs angle of attack. The values have been obtained using Richardson extrapolation from the medium- and fine-grid results[25]:

$$C_{L_{\text{exact}}} \cong C_{L_{\text{fine}}} + \frac{C_{L_{\text{fine}}} - C_{L_{\text{medium}}}}{r^p - 1}$$

where the grid-refinement ratio r is equal to 2 and a conservative estimate of the convergence order $p = 2.2$ has been used. In Fig. 14, the pressure coefficient at the wall is presented. Increasing the angle of attack, the suction peak at the airfoil leading edge increases

Table 4 List of the thermodynamic freestream conditions considered for the parametric study and corresponding aerodynamic performance

			Isentrope S1			
p_∞/p_c	1.054	1.058	1.068	1.077	1.088	1.103
ρ_∞/ρ_c	0.920	0.950	1.00	1.05	1.10	1.15
Γ_∞	$-2.09e{-2}$	$5.76e{-1}$	1.82	3.01	3.86	4.30
C_L	0.2130	0.2680	0.2236	0.4480	0.2500	0.1036
C_L/C_D	∞	∞	∞	31.11	1.897	1.169
			Isentrope S2			
p_∞/p_c	1.062	1.068	1.077	1.087	1.099	1.115
ρ_∞/ρ_c	0.920	0.95	1.00	1.05	1.10	1.150
Γ_∞	$8.05e{-2}$	$6.41e{-1}$	1.81	2.92	3.73	4.18
C_L	0.2160	0.2282	0.2740	0.4631	0.2640	0.1037
C_L/C_D	∞	∞	∞	28.58	2.015	1.158
			Isentrope S3			
p_∞/p_c	1.068	1.074	1.083	1.094	1.107	1.123
ρ_∞/ρ_c	0.920	0.950	1.00	1.05	1.10	1.12
Γ_∞	0.143	0.680	1.78	2.86	3.64	4.11
C_L	0.2180	0.2300	0.2791	0.4732	0.2780	0.1036
C_L/C_D	∞	∞	∞	26.57	2.138	1.151
			Isentrope S4			
p_∞/p_c	1.085	1.092	1.104	1.116	1.130	1.148
ρ_∞/ρ_c	0.920	0.950	1.00	1.05	1.10	1.12
Γ_∞	0.297	0.781	1.75	2.70	3.43	3.55
C_L	0.2251	0.2383	0.2911	0.5092	0.3240	0.1039
C_L/C_D	∞	∞	∞	20.61	2.512	1.135

as well, leading to higher lift. On the other hand, the strong adverse pressure gradient at the rear part of the suction side is likely to produce boundary-layer separation, resulting in a considerable modification of the flowfield and pressure distribution. To better clarify this aspect, Navier–Stokes computations of the same problem are planned. For this series of lifting cases, the Grid Convergence Index (based on the lift coefficient) was below 1% on the fine grid and about 3% on the medium grid. Moreover, the same trends for the lift and drag coefficients were obtained on the two grids. For this reason, given the considerable amount of cases to be run, only the medium grid is retained for the remainder of this study.

The last series of results is a parametric study of the influence of the thermodynamic freestream thermodynamic conditions on the airfoil performance. The freestream Mach number and the airfoil angle of attack are fixed to 0.85 and 1 deg, respectively, and the freestream conditions are changed at constant entropy. Four increasing entropy values, S1 to S4, are considered, and six operation points are chosen on each isentrope. The freestream values for pressure, density, and Γ are listed in Table 4.

The perfect-gas flow ($\gamma = 1.4$) at the same angle of attack and freestream Mach number is characterized by two shocks, located at about 85% of the chord on the suction side and 63% on the pressure side. The computed lift coefficient, drag coefficient, and lift-to-drag ratio are (on the medium grid)

$$C_L = 0.3730, \qquad C_D = 5.793 \times 10^{-2}, \qquad C_L/C_D = 6.439$$

In Table 4, the aerodynamic performances for the BZT gas are also reported, for each of the considered operation points. Several comments are in order. For freestream states quite close to the transition line, a formidable increase in the lift-to-drag ratio (which tends to infinity) is observed, associated with subcritical flow conditions over the entire airfoil. In practice, however, the computed drag coefficient is not exactly zero, but takes small nonzero values, the corresponding computed lift-to-drag ratio being $\mathcal{O}(10^2)$. Increasing the freestream pressure at fixed entropy, the lift-to-drag ratio suddenly drops to finite values. Such a drop is as a result of the onset of supercritical flow, with consequent appearance of wave drag. However, if the pressure is not too large the lift-to-drag ratio is still one order of magnitude larger than in the perfect-gas case, whereas the lift coefficient is the same or higher. For example, taking $p_\infty/p_c = 1.116$ and $\rho_\infty/\rho_c = 1.05$, the following values of lift, drag, and lift-to-drag ratio are obtained:

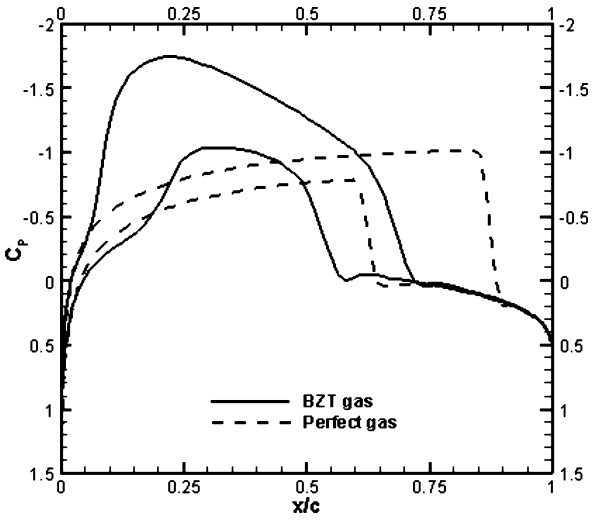

Fig. 15 Transonic flow past a NACA0012 with $M_\infty = 0.85$, $\alpha = 1$ deg. Comparison BZT gas/perfect diatomic gas.

$$C_L = 0.5090, \qquad C_D = 2.470 \times 10^{-2}, \qquad C_L/C_D = 20.61$$

The high lift coefficient is caused by the formation of an expansion shock at the suction side, close to the leading edge, which drives the pressure coefficient to values much lower than in the perfect-gas case (see wall distributions in Fig. 15); the expansion shock is followed by a gradual compression, and then by a weak compression shock, located at about 68% of the chord. Similarly, on the pressure side weak expansion and compression shocks form, at about 24 and 52% of the chord, respectively. On the other hand, flow discontinuities have limited strength and jump conditions in the vicinity of the transition line. Consequently, entropy jumps across shocks are almost negligible, and the flow is nearly isentropic. This results in an extremely low value of the wave drag and in a lift-to-drag ratio more than double with respect to the perfect-gas case. Similar considerations can be made for other operation points ($p_\infty/p_c = 1.077$, $\rho_\infty/\rho_c = 1.05$), ($p_\infty/p_c = 1.087$, $\rho_\infty/\rho_c = 1.05$), and ($p/p_c = 1.094$, $\rho/\rho_c = 1.05$). For all of the preceding cases, $\Gamma_\infty \cong 3$. In the following, we name this narrow range of particularly favorable flow conditions the BZT supercritical regime. We also remark that, choosing freestream conditions closer to the saturation curve, a larger portion of the flow falls within the inversion zone. This leads to lower drag values when compared to flows characterized by higher freestream entropy. On the other hand, significant BZT effects imply a smaller region of supercritical flow and, consequently, lower values of lift. And in fact, inspecting Table 4, it appears that for high-pressure operation points, C_L increases from isentrope S1 to isentrope S4, whereas C_L/C_D decreases. Finally, for operation points characterized by higher freestream pressure and Γ, the flow is also supercritical, but BZT effects progressively disappear, and the flow qualitatively recovers its dilute-regime behavior.

We conclude this section with a last remark concerning the equation of state used for the present study. The limits and possible sources of error related to the use of the van der Waals gas model have been discussed in Sec. II. In particular, it has been pointed out that such a model largely overpredicts the extent of the inversion zone. Thus, present results are possibly too optimistic. However, preliminary computations performed using the Martin–Hou equation of state[26] seem to confirm the present conclusions. In particular, the flow regimes just described—fully subcritical, BZT supercritical, non-BZT supercritical—have been recovered. The main differences lie in the ranges of pressures and temperatures characterizing each regime: the qualitative behavior for each regime is roughly the same. More detailed computations with the Martin–Hou equation of state are currently in progress.

V. Conclusions

The present study represents a preliminary step toward the design of dense gas organic Rankine cycles. In such cycles, dense gas effects, and in particular Bethe–Zel'dovich–Thompson (BZT) phenomena, are exploited in order to reduce losses caused by wave drag and shock/boundary-layer interactions in the expansion stage. Realization of BZT organic Rankine cycles depends on the possibility of finding a practical tradeoff between high turbine efficiency associated with dense gas effects and an adequate cycle power output. The last issue, in particular, requires the operation of the turbine with high temperature jumps, whereas the thermodynamic region where BZT effects appear (called the inversion zone) is of quite limited extent. Consequently, a compromise solution has to be found, allowing the flow to evolve only partially within the BZT region. In the present work, a detailed numerical study of transonic dense gas flows past a simplified configuration, represented by an isolated NACA0012 airfoil, has been provided. For such a configuration, a tradeoff has to be established between high lift and low drag. In particular, the objective of the study was to investigate how the freestream thermodynamic and kinematic conditions affect the airfoil aerodynamic performance, for example, lift and lift-to-drag ratio, and to explore for the first time the possibility of operating the system at freestream conditions not necessarily close to the inversion zone (which is necessary to achieve high lift) while ensuring high system efficiency, that is, high lift-to-drag ratios.

The computations have been performed using a recently developed numerical code for the solution of the two-dimensional Euler equations closed by the van der Waals equation of state for polytropic gases. The code uses a third-order centered approximation of the convective fluxes. Firstly, a detailed flowfield analysis has been provided for three nonlifting cases, and the differences with perfect-gas flow at the same conditions have been highlighted. BZT flow is characterized by an uncommon Mach variation along the airfoil and by the formation of nonclassical waves. Then, a parametric study of the influence of freestream kinematic and thermodynamic conditions has been performed. For freestream thermodynamic states sufficiently close to the inversion zone, a completely shock-free flow can be obtained, leading to a considerable increase in the airfoil performance (wave drag is completely suppressed), albeit accompanied by a reduction in lift with respect to the perfect-gas case. The lift could be increased by raising the airfoil angle of attack, but doing so large adverse pressure gradients appear at the airfoil suction side, which could deteriorate the viscous performance of the airfoil. More promising results have been obtained for operation points lying sufficiently far from the inversion zone so that supercritical flow is established, but sufficiently close to allow significant BZT effects. In such regimes, a significant reduction of the wave drag is observed, whereas the lift coefficient remains equal or even increases, with respect to the perfect-gas cases. Drag reduction is caused by the fact that flow discontinuities having jump conditions in the vicinity of the inversion zone are much weaker than normal. This benefits the inviscid performance of the airfoil, but is also expected to improve its viscous performance, as adverse pressure gradients caused by strong shocks are almost suppressed. This could in particular alleviate losses caused by shock/boundary-layer interactions.

In summary, the present results suggest that the choice of upstream conditions within or very close to the $\Gamma = 0$ line [i.e., $\Gamma = \mathcal{O}(\Delta v)$] is not only not mandatory in order to improve airfoil performance, as suggested in previous studies,[10–12] but also not optimal. Specifically, present computations, based on the van der Waals gas model, show that optimal aerodynamic performance (i.e., the best compromise between high lift and low drag) is obtained for $\Gamma = \mathcal{O}(1)$, more precisely, $\Gamma \approx 3$. This is of great importance, in light of the design of BZT organic Rankine cycles. In fact, it suggests the possibility of enlarging the operation range of the expansion stage without losing the benefits related to dense gas effects and increasing the global cycle efficiency at the same time.

References

[1]Thompson, P. A., "A Fundamental Derivative in Gas Dynamics," *Physics of Fluids*, Vol. 14, No. 9, 1971, pp. 1843–1849.

[2]Cramer, M. S., and Kluwick, A., "On the Propagation of Waves Exhibiting Both Positive and Negative Nonlinearity," *Journal of Fluid Mechanics*, Vol. 142, 1984, pp. 9–37.

[3]Cramer, M. S., "Shock Splitting in Single-Phase Gases," *Journal of Fluid Mechanics*, Vol. 199, 1989, pp. 281–296.

[4]Lambrakis, K. C., and Thompson, P. A., "Existence of Real Fluids with a Negative Fundamental Derivative Γ," *Physics of Fluids*, Vol. 15, No. 5, 1972, pp. 933–935.

[5]Thompson, P. A., and Lambrakis, K. C., "Negative Shock Waves," *Journal of Fluid Mechanics*, Vol. 60, 1973, pp. 187–208.

[6]Cramer, M. S., "Negative Nonlinearity in Selected Fluorocarbons," *Physics of Fluids A*, Vol. 1, No. 11, 1989, pp. 1894–1897.

[7]Cramer, M. S., "Nonclassical Dynamic of Classical Gases," *Nonlinear Waves in Real Fluids*, Springer-Verlag, Berlin, 1991, pp. 91–145.

[8]Menikoff, R., and Plohr, B. J., "The Riemann Problem for Fluid Flow of Real Materials," *Review of Modern Physics*, Vol. 61, No. 1, 1989, pp. 75–155.

[9]Cramer, M. S., and Best, L. M., "Steady, Isentropic Flows of Dense Gases," *Physics of Fluids* A, Vol. 3, No. 1, 1991, pp. 219–226.

[10]Cramer, M. S., and Tarkenton, G. M., "Transonic Flows of Bethe-Zel'dovich-Thompson Fluids," *Journal of Fluid Mechanics*, Vol. 240, 1992, pp. 197–228.

[11]Monaco, J. F., Cramer, M. S., and Watson, L. T., "Supersonic Flows of Dense Gases in Cascade Configurations," *Journal of Fluid Mechanics*, Vol. 330, 1997, pp. 31–59.

[12]Brown, B. P., and Argrow, B. M., "Application of Bethe-Zel'dovich-Thompson Fluids in Organic Rankine Cycles," *Journal of Propulsion and Power*, Vol. 16, No. 6, 2000, pp. 1118–1124.

[13]Batton, W. D., and Hunt, J. H., "Turbines: the Most Likely Benefactor of BZT Fluids," Barber-Nichols, Inc., Technical Paper, URL: http://www.barber-nichols.com/literature.htm [cited 1 March 2002].

[14]Argrow, B. M., "Computational Analysis of Dense Gas Shock Tube Flow," *Shock Waves*, Vol. 6, No. 4, 1996, pp. 241–248.

[15]Brown, B. P., and Argrow, B. M., "Nonclassical Dense Gas Flows for Simple Geometries," *AIAA Journal*, Vol. 36, No. 10, 1998, pp. 1842–1847.

[16]Fergason, S. H., Ho, T. L., Argrow, B. M., and Emanuel, G., "Theory for Producing a Single-Phase Rarefaction Shock Wave in a Shock Tube," *Journal of Fluid Mechanics*, Vol. 445, 2001, pp. 37–54.

[17]Martin, J. J., and Hou, Y. C., "Development of an Equation of State for Gases," *AIChE Journal*, Vol. 1, No. 2, 1955, pp. 142–151.

[18]Emanuel, G., "Assessment of the Martin-Hou Equation for Modelling a Nonclassical Fluid," *Journal of Fluids Engineering*, Vol. 61, No. 4, 1994, pp. 883, 884.

[19]Huang, Y., Cinnella, P., and Lerat, A., "A Third-Order Accurate Centered Scheme for Turbulent Compressible Flow Calculations in Aerodynamics," *Numerical Methods for Fluid Dynamics*, Vol. 6, Will Print, Oxford, 1998, pp. 355–361.

[20]Cinnella, P., and Congedo, P. M., "A Numerical Method for Dense Gas Flows," *AIAA Journal* (submitted for publication); also AIAA Paper 2004-2137, June–July 2004.

[21]Jameson, A., Schmidt, W., and Turkel, E., "Solutions of the Euler Equations by Finite Volume Methods Using Runge–Kutta Time-Stepping Schemes," AIAA Paper 8l-l259, June 1981.

[22]Napolitano, M., Bonfiglioli, A., Cinnella, P., De Palma, P., and Pascazio, G., "Future Directions for Computing Compressible Flows: Higher Order Centering Versus Multidimensional Upwinding," *Frontiers of CFD 2001*, edited by A. Caughey and M. Hafez, World Scientific, Singapore, 2002, pp. 113–127.

[23]Rezgui, A., Cinnella, P., and Lerat, A., "Third-Order Finite Volume Schemes for Euler Computations on Curvilinear Meshes," *Computers and Fluids*, Vol. 30, No. 7–8, 2001, pp. 875–901.

[24]Guardone, A., and Vigevano, L., "Roe Linearization for the van der Waals Gas," *Journal of Computational Physics*, Vol. 175, No. 1, 2002, pp. 50–78.

[25]Roache, P. J., *Verification and Validation in Computational Science and Engineering*, Hermosa, Albuquerque, NM, 1998.

[26]Cinnella, P., Congedo, P. M., and Laforgia, D., "Investigation of BZT Transonic Flows Past an Airfoil Using a 5th Power Virial Equation of State," *Proceedings of the 4th European Congress on Computational Methods in Applied Sciences and Engineering* [CD-ROM], Vol. 1, Univ. of Jyvaskyla, Jyvaskyla, Finland, 2004.

J. Bellan
Associate Editor